On the use of advanced measurement techniques for characterization of bond behavior in FRP-masonry components

Bahman Ghiassi[1†], Daniel V. Oliveira[2], Paulo B. Lourenço, [3]

ISISE, Universidade do Minho, Departamento de Engenharia Civil
Azurém, P - 4800-058 Guimarães, Portugal

ABSTRACT

Fiber reinforced materials are frequently used as externally bonded reinforcement (EBR) for structural enhancement of concrete and masonry structures. Significant progress has been achieved in the last years regarding experimental investigation and computational modeling of the debonding phenomenon and damage in FRP-strengthened masonry elements. However, aspects such as failure initiation, interfacial damage propagation and localization, three-dimensional nature of the bond behavior, effective bond length and strain distributions along the reinforcement as well as nondestructive bond quality monitoring are still open issues. This paper shows how these aspects can be monitored and characterized by means of three full-field measurement techniques including Infrared (IR) thermography, Digital Image Correlation (DIC) and Acoustic Emission (AE).

1. INTRODUCTION

Fiber reinforced materials are frequently used as externally bonded reinforcement (EBR) for structural enhancement of concrete and masonry structures, with advantages such as low weight to strength ratio and versatility in application. The effectiveness of EBR techniques is intrinsically dependent on the bond behavior between the composite material and the masonry substrate. It is known that the environmental conditions can cause bond degradation and FRP delamination in the interfacial region, which affect the performance of the strengthened structure. FRP delamination may also occur due to poor workmanship. Fully understanding the involved strain and stress transfer mechanisms and fracture progress in the interfacial region (bond) is thus crucial for design and structural health assessment. In this regards, use of advanced non-destructive qualitative and quantitative bond assessment methods seems interesting for bond performance assessment in both laboratory tests and on-site structural health monitoring purposes.

Significant progress has been achieved in the last years regarding experimental investigation and computational modeling of the debonding phenomenon and damage in FRP-strengthened masonry elements, see e.g. (Oliveira et al. 2011, Valluzzi et al. 2012, Ghiassi et al. 2012, Carrara et al. 2013). However, aspects such as failure initiation, interfacial damage

[1] Postdoctoral researcher
[†] Corresponding author (bahmanghiassi@civil.uminho.pt)
[2] Associate Professor
[3] Professor

propagation and localization, three-dimensional nature of the bond behavior, effective bond length and strain distributions along the reinforcement as well as nondestructive bond quality monitoring are still open issues. This paper shows how these aspects can be monitored and characterized by means of three advanced measurement techniques: (a) Infrared (IR) thermography; (b) Digital Image Correlation (DIC); (c) Acoustic Emission (AE). Although some of these techniques (such as DIC) have been used extensively used other fields of structural mechanics, it should be noted that in most cases, the progress and development of these techniques are not yet advanced and there are still open issues (such as in AE and IR thermography techniques). On the other hand, the use of these techniques for quantitative characterization of bond is quite new, and in some cases (such as AE) this work is among the first research studies.

GFRP-strengthened brick specimens are prepared and exposed (after curing) to different environmental conditions in a climatic chamber. The specimens are taken from the climatic chamber after different exposure periods for qualitative and quantitative characterization of the bond degradation. Visual inspection is initially performed on the specimens for detection of any visible FRP delamination or color changes. Then, IR thermography test is performed on the specimens for detection of any environmentally induced FRP delaminations. The size of FRP delaminations are also quantitatively measured with the aim of advanced IR analysis algorithms. Single-lap shear bond tests are finally performed on the specimens for quantitatively characterization of the bond degradation. The AE and DIC techniques are used during the debonding tests for characterization of the fracture progress and measurement of surface deformation. Here, a review of the experimental results obtained from IR thermography, DIC and AE techniques are presented and discussed and the results obtained from mechanical tests are presented elsewhere (Ghiassi 2013a).

2. ADVANCED MEASUREMENT TECHNIQUES

Despite the extensive experimental and theoretical investigations conducted on the bond behavior between composite materials and concrete or masonry substrates, development and utilization of non-destructive and full-field measurement techniques to monitor the bond quality condition or active fracture mechanisms during debonding have received less attention (Ghiassi 2013a).

2.1

Visual inspection and hammer tapping are the most widely used in-situ non-destructive testing methods for bond characterization in FRP-strengthened elements. Methods such as digital image correlation (DIC), infrared (IR) thermography and acoustic emission (AE) testing have recently received more attention and seem interesting the laboratory and in-situ characterization of bond and. A brief description of these techniques is presented in this section and the reader is referred to the given references for a more detailed description of each technique.Digital Image Correlation

Several interferometric and white-light optical methods have been proposed and developed in experimental solid mechanics for displacement or strain measurements over an entire region of interest (ROI) (Sutton et al. 2009). Among these techniques, non-interferometric methods based on image processing, such as the DIC, have been increasingly used (Pan et al. 2009, Sousa et al. 2011, Xavier et al. 2012). However, only a few studies can be found using these techniques for investigating the interfacial bond behavior, see e.g. (Carloni and Subramaniam 2012, Ghiassi et al. 2013b). These techniques contrast with conventional strain gauges or extensometers by the fact that they provide full-field data and

are contact-free.

The DIC technique provides full-field displacements of an object by comparing the similarity between images recorded, at least, at two different mechanical states. The strain field can then be obtained from the derivation of the displacement field. The region of interest (ROI) must have a speckled pattern, which is typically obtained by spray or airbrush painting. A suitable balance between the ROI and average size of white-to-dark spots must be achieved in order to enhance the displacement spatial resolution (small aperture) associated to the DIC measurements.

This technique can be used during debonding tests for obtaining the distribution of strains on the FRP surface and investigating the three-dimensional aspects of the bond behavior such as transversal strains or the changes of bond-slip behavior along FRP width (Ghiassi et al. 2013). The full-field strain distribution can also be used for characterization of bond-slip laws to be used in numerical modeling approaches.

2.2 Infrared Thermography

The IR thermography method has been extensively used in the last years for detection and evaluation of defects in FRP bonded components (Lai et al. 2013, Tashan and Al-mahaidi 2012). Applications are mostly focused on the qualitative assessment and the localization of the defects. However, once the defects have been located, it is interesting to characterize them quantitatively in order to evaluate the performance of the structure. This has led to development of several quantitative measurement approaches (Maldague 2001). Quantitative IR thermography methods have been adopted in the last years for bond quality assessment purposes in FRP bonded components (Lai et al. 2013, Ghiassi et al. 2014a).

Infrared thermography methods can be divided into passive infrared thermography (PIT) and active infrared thermography (AIT) techniques. The difference between these two methods is that external surface heating is required in the AIT, while in the PIT no external heating is applied and the natural surface temperature of the specimen is monitored and analyzed. In other words, in AIT, heat energy is applied to the specimen and the surface response to this energy is analyzed for localization and evaluation of the defects or material discontinuities. Alternatively, the surface temperature of the specimen at ambient conditions is monitored in PIT without application of any heat energy. Suspicious defects and flaws can be distinguished from abnormal temperature profile on the surface. Special care should be taken in interpretation of the results since anomalous thermal gradients can also be produced due to non-uniform heating or reflection effects.

Use of IR thermography for bond quality characterization is based on the principle that the heat flux is transmitted at different rates in materials with different thermal properties (Maldague 2001). In an FRP-strengthened element, any defect or delamination in the interfacial region changes the thermal properties in that area. Therefore, if a heat flux is applied to the surface of an FRP-bonded element, the heat will be transferred with a different rate in the defected areas with respect to the perfectly bonded regions. This leads to the appearance of hot or cold spots in thermal images depending on the heat observation method.

2.3 Acoustic Emission

Acoustic Emissions (AE) are high-frequency transient elastic waves that are emitted within the material during local stress redistributions occurring during crack initiation and growth. These emissions are detected on the material's surface by means of piezoelectric transducers, pre-amplified, filtered and amplified before they are sent to the data logger. The

technique has the advantage over other damage detection techniques that it relies on detection of information which is generated by the fracture process itself and allows for on-line damage detection and assessment.

Background noise is eliminated using a minimum amplitude threshold. An AE hit with a predefined duration is recorded when the threshold is exceeded. For each AE hit, a number of parameters (e.g. arrival time, amplitude, count, duration, energy) and the waveform itself are recorded. The amount of detected AE hits and energy is influenced by the applied hardware and software settings, thus software defined parameters (e.g. threshold and sampling frequency) should be kept constant for subsequent tests.

The recorded acoustic emissions hold information on the fracture process which produced them. Basic AE hit counting, taking into account the cumulative or average number of AE hits or emitted AE energy, has successfully been used for damage assessment in rock, concrete and masonry (Grosse and Ohtsu 2008, Verstrynge et al. 2009) and recently has been used for FRP-masonry systems as well (Ghiassi 2013a, Ghiassi et al. 2014b). It is generally observed that micro-cracks generate a large amount of small amplitude emissions, while AE emissions from macro-cracks are fewer but have higher amplitude. Based on this observation, the b-value is applied in seismic analysis to characterize the fracture process by means of the slope of the amplitude distribution. Instead of the seismic b-value, an improved b-value (Ib-value), in which the number of AE data taken into account is set before calculation, is usually applied for AE applications in concrete and rock. More advanced signal-based analysis takes into account the complete AE signal allowing characterization of the fracture modes (Grosse and Ohtsu 2008). Therefore, high sampling rates and the use of broadband AE sensors is required. The needed dedicated signal processing and interpretation can become time-consuming for large data sets. Signal-based analysis has known limited application in concrete and masonry, due to the high attenuation and distortion of the AE wave caused by the heterogeneity of the material, especially in case of masonry.

3. APPLICATION TO BOND CHARACTERIZATION

The application of the above mentioned techniques in bond performance assessment during the debonding tests and after aging in environmental conditions is investigated in this section. For this reason, GFRP-strengthened brick specimens are prepared and exposed (after curing) to environmental conditions in a climatic chamber. Five specimens are taken from the climatic chamber after each 50 cycles of exposure for characterization of the bond degradation according to the protocol shown in Figure 1, (Ghiassi 2013a). Visual inspection is initially performed on the specimens for detection of any visible FRP delamination or color changes. Then, IR thermography test is performed on the specimens for detection of the environmentally induced FRP delaminations. The size of FRP delaminations are also quantitatively measured with the aim of advanced IR analysis algorithms. Single-lap shear bond tests are finally performed on the specimens for quantitatively characterization of bond degradation. The AE and DIC techniques are used during the debonding tests for characterization of the fracture progress and measurement of surface deformation. A review of the experimental test program and tests setup is given in this section.

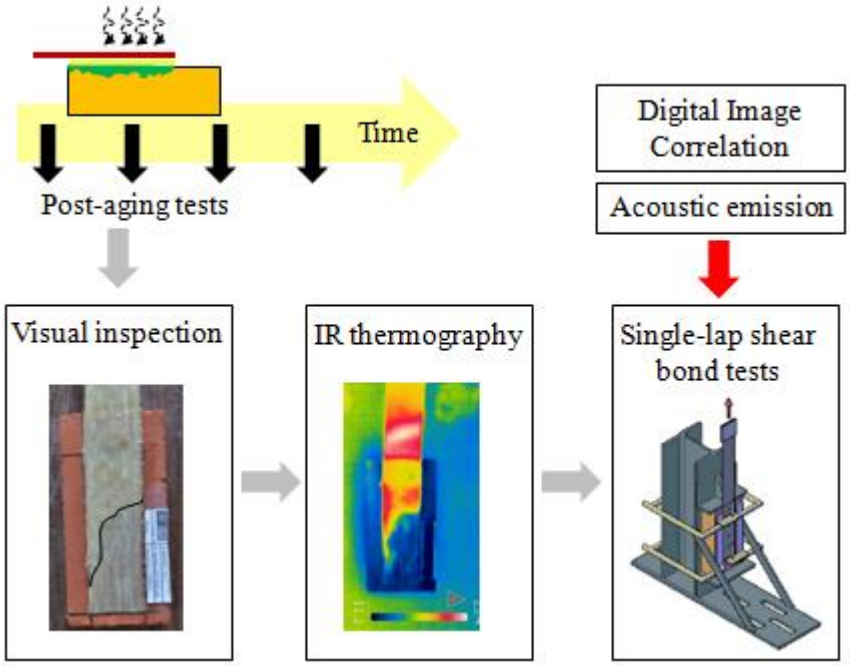

Figure 1 – Testing program.

3.1 Materials and specimens

The specimens consisted of single bricks strengthened with GFRP composites prepared following the wet lay-up procedure. Solid clay bricks with dimensions of 200×100×50 mm were used as substrate. The GFRP sheets with 50 mm width were applied on the bricks' surfaces with a bonded length of 150 mm leaving a 40 mm unbonded part near the loaded end. The bricks were dried in the oven before application of the GFRP sheets. Then, a two-part epoxy primer was applied to the brick's surface for preparation of the substrate surface. Finally, a two-part epoxy resin was used as the matrix for the composite material. The geometrical details of the specimens are shown in Figure 2.

The mechanical characterization tests are obtained according to relevant test standards and has been reported elsewhere (Ghiassi et al. 2013).

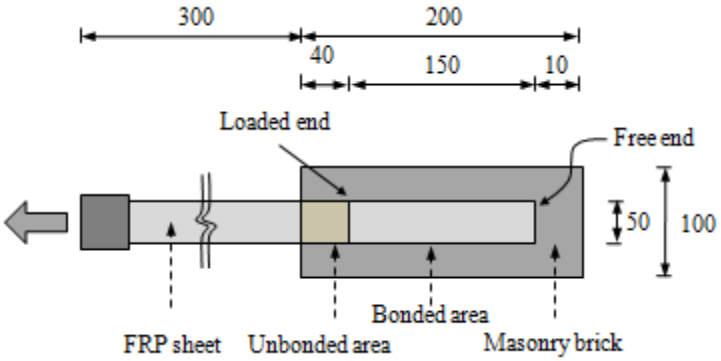

Figure 2 – Geometrical details of the GFRP-strengthened brick specimens (all units in mm).

3.2 Accelerated ageing tests

The specimens were exposed to two different accelerated hygrothermal conditions in a climatic chamber, see Figure 3. The aim was to investigate the applicability of IR thermography method in detection of environmental induced delaminations and interfacial defects.

In the first exposure, HT, the specimens were exposed to 6 hr temperature cycles from +10℃ to +50℃ and constant relative humidity of 90%. In each cycle, the temperature was kept constant at +10℃ for 2 hr. The temperature was then increased to +50℃ in 1 hr, followed by 2 hr constant temperature at +50℃. Finally, the temperature was decreased again to +10℃ in 1 hr resulting in 6 hr cycles of exposure. In the second exposure, FT, the specimens were exposed to temperature cycles from -10℃ to +30℃ and, again, constant relative humidity of 90%. The specimens were subjected to a total of 200 cycles in each exposure condition. The specimens were inspected visually and tested with IR thermography technique after each fifty cycles of exposure to investigate the applicability of the test method in obtaining the environmental induced interfacial defects and delaminations.

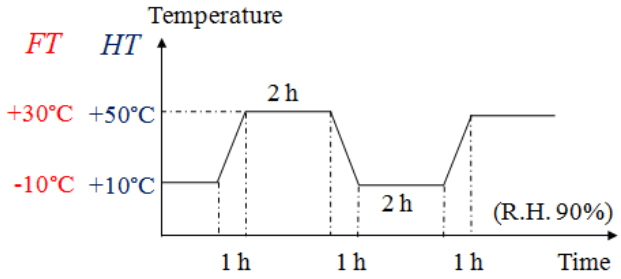

Figure 3 – Environmental exposures.

3.3 Delaminations tests setup

Single-lap shear bond tests were performed using a closed-loop servo-controlled testing machine with maximum load capacity of 50 kN. A rigid supporting steel frame was used to support the specimens appropriately and avoid misalignments in the load application, see Figure 4. The specimens were placed on the steel frame and firmly clamped. The specimens were pulled monotonically with a speed rate of 5 µm/sec under displacement control conditions with reference to the LVDT placed at the loaded end of the FRP composite. The resulting load was measured by means of a load cell.

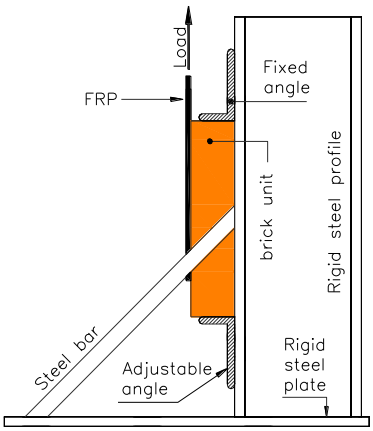

Figure 4 –Schematic of the delamination tests setup.

3.4 IR thermography tests setup

The tests were performed with a FLIR ThermaCAM T400 infrared camera with spectral range of 7.5-13 μm and thermal sensitivity of <0.07ºC. Thermal videos were recorded at the rate of 9 frames/sec, at the cooling stage. The recorded videos were converted into sequential 8-bit digitized photos of 320×240 pixels for each recorded frame. In 8-bit formatting system each pixel has a value between 0 to 255, which represents different colors and temperature variations in a linear scale. The data for each test was converted into 3D matrices with the size of 320×240×*t*, where the third dimension of the matrix represents time. The temperature decay through time and analysis of the thermal images were then performed through a Matlab code specially developed. Two lamps with a maximum power of 2000 W were used as heating sources. The lamps were placed at 500 mm distance from the specimens, for 30 seconds. The position and duration of the heat exposure were optimized to obtain the best uniform heat distribution on the specimens' surfaces.

3.5 DIC tests setup

For application of the DIC technique in fracture characterization, the specimens were prepared by applying a speckle pattern on the Region of Interest (ROI), produced by applying a thin coating of white matt followed by a spread distribution of black dots using spray paint. The ARAMIS DIC-2D (2009) software by GOM was used in this work. The measurement system was equipped with an 8-bit Baumer Optronic FWX20 camera coupled with a Nikon AF Micro-Nikkor 200mm *f*/4D IF-EDlens. The optical system was positioned facing the surface of the specimens during the delamination tests, see Figure 5. A laser pointer was used to guarantee the correct alignment of the camera with regards to the specimen. The working distance (defined between the target surface and the support of the cameras) was set about 1.8 m leading to a conversion factor of 0.037 mm.pixel^{-1}. The aperture of the lens was completely open (minimum depth of field) in order to focus the image on the specimen's surface. The lens aperture was then closed to *f*/11 in order to improve the depth of field during the testing. The shutter time was set to 5 ms. The light source was finally adjusted in order to guarantee an even illumination of the target surface and to avoid over-exposition. The typical resolution of the measurements was in the range of 10^{-2} mm and 0.02-0.04 % for displacement and strain evaluation, respectively.

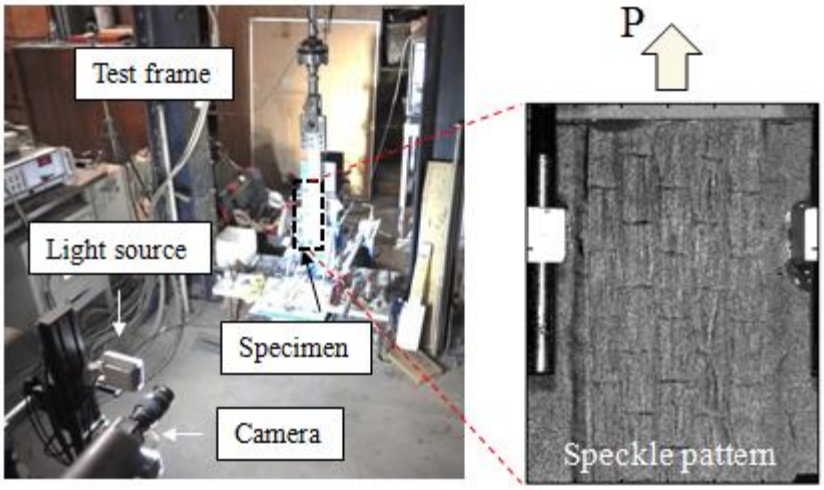

Figure 5 – Digital image correlation test setup

3.6 Acoustic emission tests setup

Acoustic emissions were monitored, during the delamination tests, using a 4-channel Vallen AMSY-5 system with 150-500 kHz operation frequency and 5 MHz sampling rate. Four 150 kHz resonance sensors were attached to opposite sides of the bricks by means of hot melt glue, see Figure 6. The preamplifier gain was set to 34 dB with a fixed threshold level of 40 dB and pencil lead breaks were used for system calibration. To calculate the AE energy, the AE signal is squared and integrated and the energy unit (eu) is given by $1eu = 10^{-14}V^2s$.

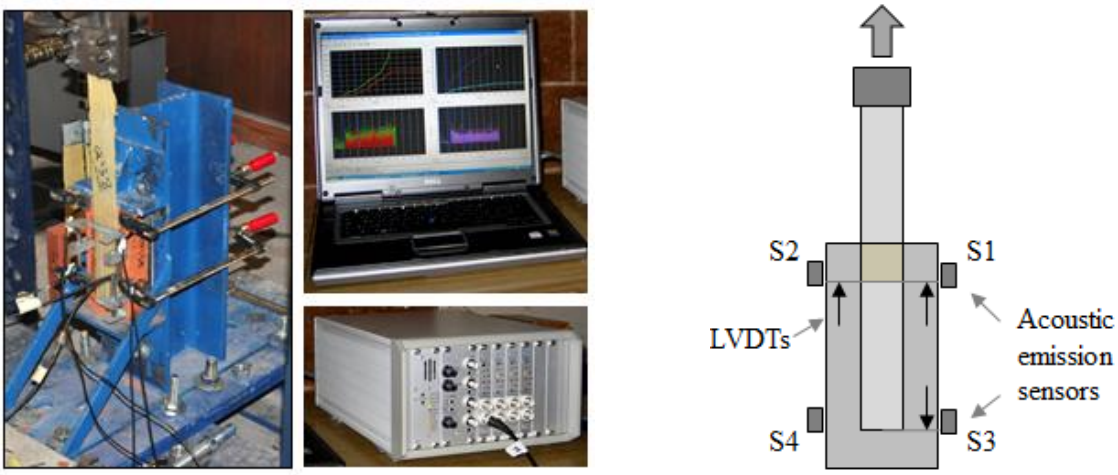

(a) (b)

Figure 6 – Acoustic emission tests: (a) test setup; (b) test instrumentation.

4. RESULTS AND DISCUSSION

4.1 IR thermography tests

For investigating the applicability of IR thermography technique in the detection of environmentally induced delamination, the GFRP-strengthened brick specimens exposed to accelerated hygrothermal conditions, are inspected with this method after different periods of exposure. For each exposure period, after localization of interfacial delamination, its size and boundaries are evaluated quantitatively and the results are presented next.

As expected, FRP delamination is observed in some specimens after exposure to hygrothermal conditions. In general, relatively large FRP delaminations were observed in the specimens exposed to HT conditions. On the contrary, the specimens exposed to FT conditions have very small delamination. As an example, the corresponding thermal images and detected FRP delaminated areas, from IR thermography tests, for the specimens exposed to HT conditions are presented in Figure 7. It can be observed that the FRP delamination is progressively increased with the exposure time.

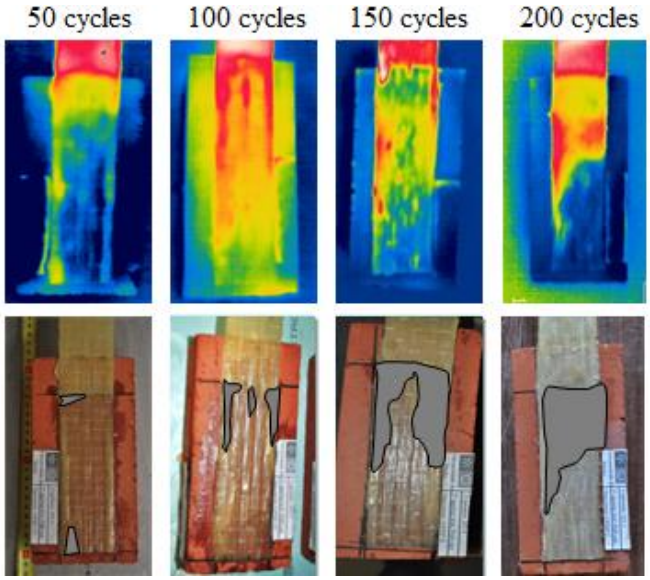

Figure 7 – Qualitative assessment of delaminated areas after different periods of exposure to HT conditions, using IR tomography.

Once the delamination is localized, the captured thermograms are analyzed according to the two-point inflection method to quantify the FRP delaminated areas. For this reason, the temperature profiles are obtained along the bonded length at longitudinal sections (trying to obtain the edge lines and the center line of the delamination area), see e.g. Figure 8. Then, the temperature profiles near the detached areas are fitted with a 4th order polynomial curve (Lai et al. 2013; Ghiassi et al. 2014a). The inflection point of the estimated curve is selected as the boundary of the FRP delaminated area.

The observed delaminations are evaluated quantitatively in all the specimens according to the described methodology. Figure 9 presents the results as the average of five specimens in terms of the remaining bonded area normalized to the initial bonded area. It can be observed that the delamination in the specimens exposed to HT exposure is relatively large (23% reduction of bonded area after 200 cycles). Meanwhile, the reduction in the bonded area in the specimens exposed to FT conditions is very limited (2% after 200 cycles). Moreover, a sudden increase in delamination rate can be observed after 100 cycles of exposure to HT conditions, followed by some stabilization.

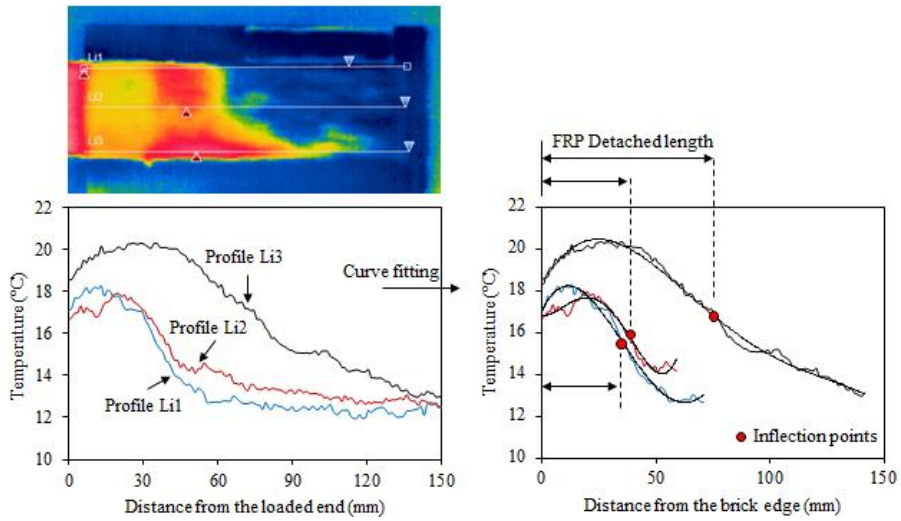

Figure 8 – Temperature profiles and quantitative assessment of delaminated areas in a specimen exposed to 200 cycles of HT exposure.

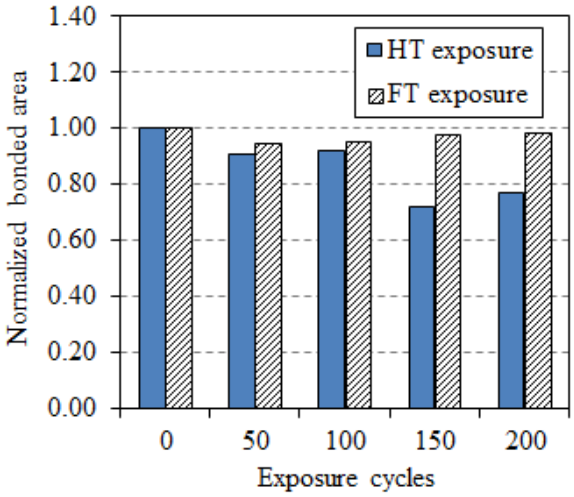

Figure 9 – Reduction of the bonded area with exposure cycles.

The observed FRP delaminations can be attributed to the thermal incompatibility between materials. However, moisture can also play an important role in weakening the bond strength. The thermal expansion coefficient of clay bricks is in the order of 5×10^{-6}/℃ (Kralj et al. 1991). The thermal expansion coefficient of E-glass fibers is similar to the clay bricks, while for the epoxy resin is in the range of $3\sim5\times10^{-5}$/℃ (CNR-DT 200 2004). This one-order magnitude difference of thermal expansion coefficient between epoxy resin and glass fibers/bricks produces large interfacial thermal stresses at the fiber/epoxy and brick/epoxy interfaces. Cyclic temperature conditions induce thermal fatigue and may cause FRP delaminations from the brick surface during the environmental exposure. The smaller delaminated areas observed in the specimens exposed to the FT conditions, can be explained with the fact that the thermal expansion coefficient of epoxy resins is much lower at low and negative temperatures (Dohnalek 2006).

The results show the applicability of IR thermography technique bond health assessment in durability studies for research purposes as well as onsite monitoring in cases in which the FRP surface is not protected with any renderings. However, application of this technique for far field assessments or in cases in which a protective rendering mortar is applied on the FRP surface remains open requiring further investigations.

4.2 DIC tests

The typical force-slip response of the specimens obtained from delamination tests is shown in Figure 10(a). The distribution and evolution of strains with load increment along the bonded length, determined from the DIC measurements, is also presented, see Figure 10(b). The strain contours are corresponding to the distribution of the longitudinal strain on the FRP surface at different load levels, denoted by A ($0.1P_u$), B($0.5P_u$), C($0.8P_u$), and D(P_u). It can be observed that the DIC provides the possibility of monitoring the evolution of strains during the delamination tests. A light unsymmetrical distribution of strains can be observed at point D, Figure 10(b), which can be attributed to the unsymmetrical loading of the specimens during the test or inhomogeneous bond characteristics along the width of the selected specimen. It should be noted that detection of the above mentioned unsymmetrical strain distribution is an advantage of using full-field measurement techniques in comparison to conventional use of strain gauges. Having the full-field distribution of strains, the strain profiles can be extracted at any load step and location. As an example, the longitudinal and

transverse strains profiles obtained in the middle of FRP are shown in Figure 10 (c, d). The significant transversal strains appear near the loaded end at high load levels being an evidence of the three-dimensional nature of the debonding phenomenon. It can be observed that the strain values increase suddenly moving forward from point C to D which is due to the initiation of debonding and crack propagation along the FRP bonded length.

The longitudinal strain profiles are then approximated with a nonlinear expression by performing a regression analysis, see Figure 11(a). It can be seen that the bonded area consists of three main regions. The FRP is fully debonded from the substrate near the loaded end. This is followed by a stress transfer zone, and after that no stress is transferred to the substrate. The length of the stress transfer zone, about 30 mm in this case (average of three tests), is the effective bond length. The longitudinal strain profiles can also be used for obtaining the bond-slip laws which are used as the input for numerical modeling approaches (Ghiassi et al. 2013b).

In fact, the bond stress and slip distribution within the bonded length at each load level can be obtained as follows:

$$\tau(x) = t_f E_f \frac{d\varepsilon_f}{dx} \quad (1)$$

$$s(x) = \int \varepsilon_f dx \quad (2)$$

where $d\varepsilon_f / dx$ is the gradient of FRP strain along the sheet length, E_f is the FRP elastic modulus, and t_f is the FRP thickness. Having the stress and slip distribution along the bonded length at each load level, the bond-slip law of the specimens is extracted and presented in Figure 11(b). It seems that the bond-slip curve follow a tri-linear trend with a plastic branch in the middle.

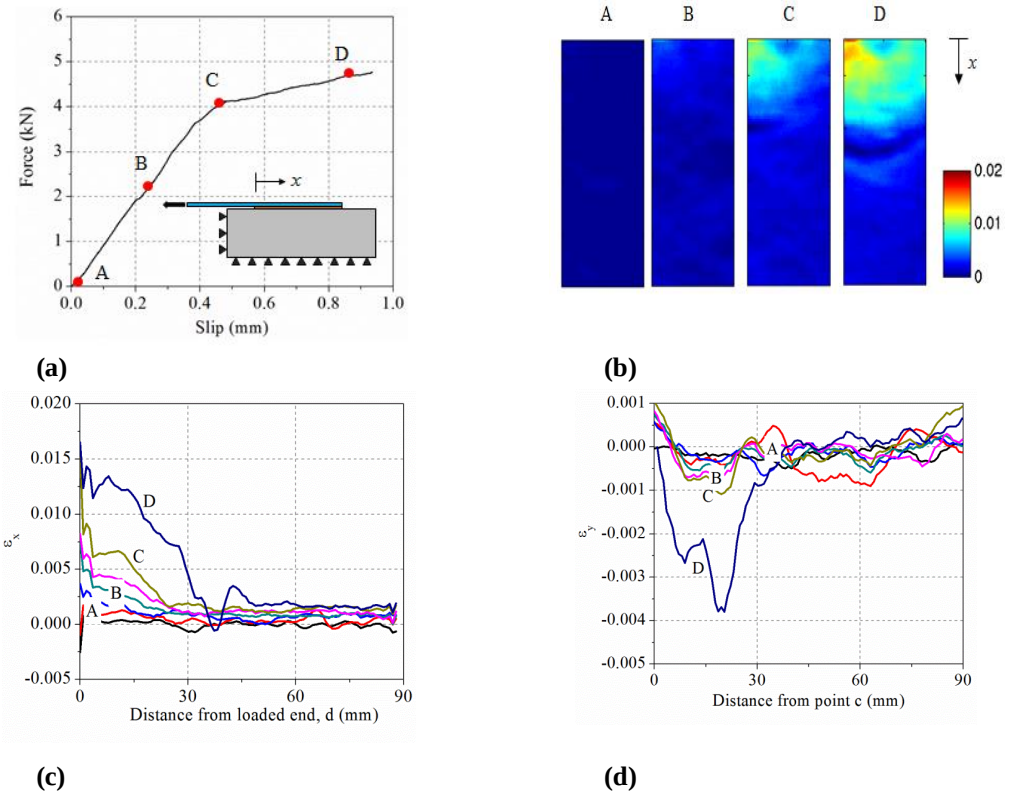

Figure 10 – (a) Typical experimental force-slip curve; (b) full-field longitudinal strains; (c) longitudinal strains along the middle of FRP; (d) transversal strains along FRP edge.

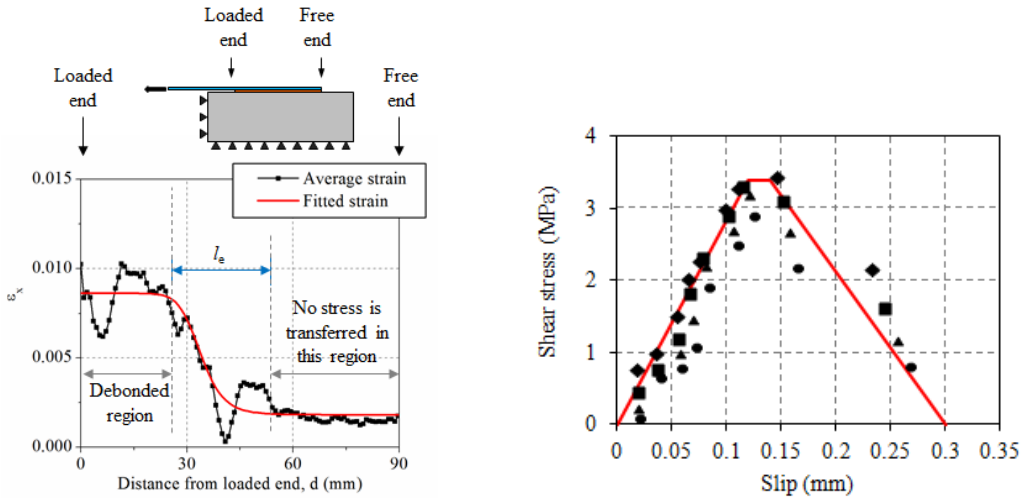

(a) **(b)**

Figure 11 – (a) Average longitudinal strain along FRP middle section and the effective bond length l_e; (b) bond-slip law.

The results show that the DIC can provide useful and additional information in comparison to conventional use of strain gauges durign the debonding tests. The full field measurements help in better understanding the debonding mechanism and fracture laws, although the need for sophisticated equipment and high expertise, limitation to the surface measurements and optical induced errors can be regarded as its disadvantages.

4.3 AE results

Typical AE results obtained from the debonding tests on GFRP-strengthened brick specimens are shown in Figure 12. The results are presented for a reference specimen with mixed cohesive/adhesive failure mode, in terms of cumulative AE energy and hits together with the force and slip development during the tests. The cumulative AE energy to hit ratio, called *E*/*h* hereafter, is also investigated and the results are presented.

Generally, the debonding phenomenon can be divided into three main regions: elastic range, micro-cracking range, macro-cracking and fracture range. In the elastic range, the system deforms without any crack generation and AE activities. The displacement measured at this stage is small being due to the elastic deformation of the FRP composite. As the applied force increases, micro-cracks appear in the interfacial region and they can be distinguished by initiation of AE activity with low emitted energies, e.g. after 100 sec of the test in Figure 12 (a, b). Since the fracture energy release due to the formation of micro-cracks is relatively small, low values of AE energies are expected in this region, see Figure 12 (a). The rate of detected AE hits is higher than the AE energy rate at this stage, resulting in a descending E/h, which indicates the formation of micro-cracks, see Figure 12 (c). As the debonding progresses, macro-cracks are formed and propagated along the interface with higher fracture energy being released. Therefore, higher AE energy is detected in this region. The cumulative AE energy increases with a stepwise pattern in which each sudden jump of energy can be correlated to a sudden fracture energy release and can thus be attributed to macro-fracture events, see Figure 12 (a, d). A sudden release of a high amount of AE energy can also be observed at the moment of full debonding, coinciding with the end of the test. The *E*/*h* ratio, Figure 12 (c), shows that each stage of the progressive debonding starts with a high rate of energy release (observed as a sudden jump in the *E*/*h* curve) and continues with a

descending rate until the end of each stage. The sudden jumps in *E*/*h* curve, in macro-fracture range, are due to the formation of macro-cracks with high energy release. Figure 12 (d) shows a clear correlation between slip increment and cumulative AE energy. This correlation can be used for predicting the FRP slip or debonding fracture energy in FRP-strengthened masonry elements.

The effect of failure mode on the AE outputs is investigated in Figure 13. A clear distinction is found between AE outputs of specimens with different failure modes. It can be observed that in the specimen with cohesive debonding the AE energy remains relatively low throughout the test, accompanied by a sudden and large amount of AE energy release and increase of *E*/*h* ratio when the debonding occurs at the end of the test, see Figure 13 (a). The observed behavior confirms the brittle and sudden nature of the cohesive debonding. Fewer peaks are observed in the *E*/*h* curve compared to the specimen with cohesive/adhesive debonding. At the end, a macro-crack with a high amount of energy release has suddenly occurred, leading to the complete debonding of the FRP. On the contrary, in the specimen with cohesive/adhesive failure a progressive release of energy is observed during the test. The high rate of energy detection shows the high number of active cracks and progressive failure during the tests. In the specimen with adhesive debonding mode, Figure 13 (b), increasing detection of AE energy is observed until the complete debonding. However, the magnitude of the detected energy is much lower than the ones detected in the specimens with cohesive failure mode. This large difference is due to the different nature and fracture properties of brick and FRP/brick interface. The specimen with adhesive failure combined with formation of a brick bulb at the free end shows a similar AE energy emission similar to the specimen with pure adhesive failure. However, a large amount of energy is released in this specimen before debonding due to the brick bulb fracture at the free end.

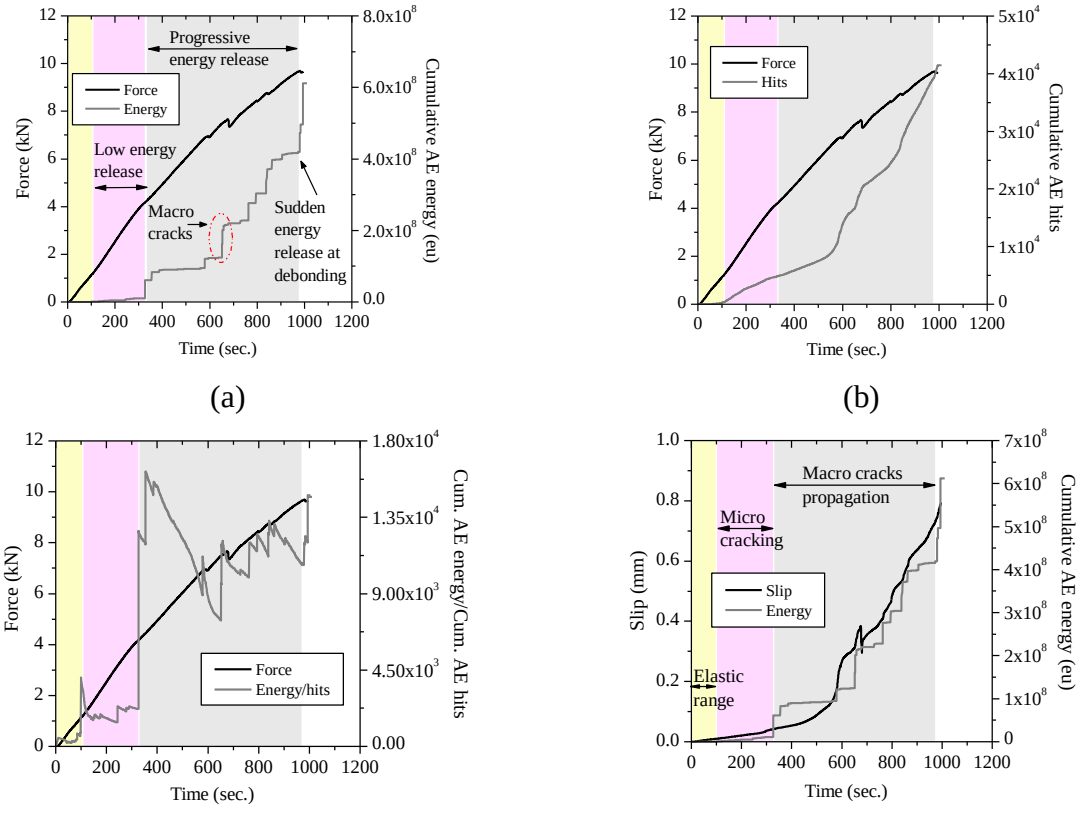

Figure 12 – Typical AE results in reference specimens: (a) force-cumulative AE energy; (b) force-cumulative AE hits; (c) force-energy/hits, E/h; (d) slip-cumulative AE energy.

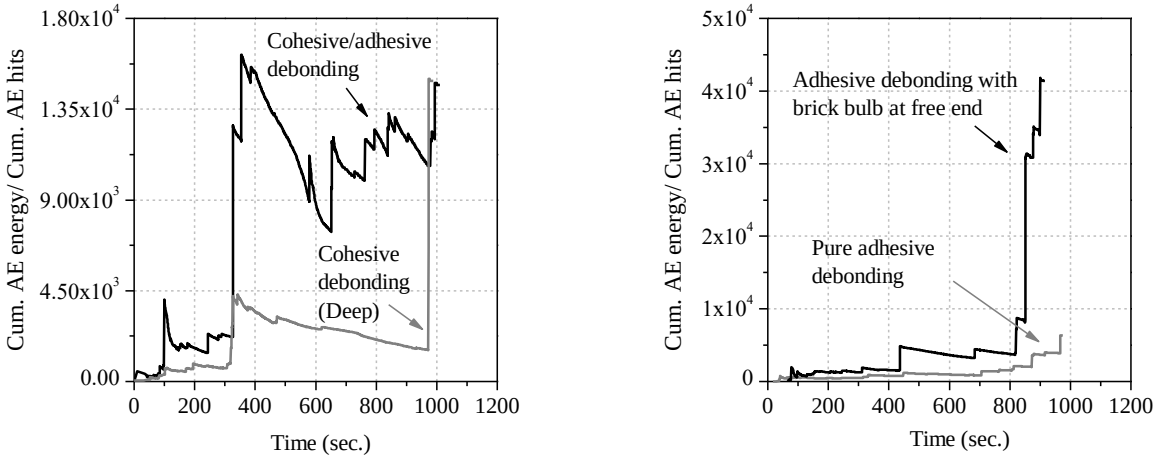

(a) (b)

Figure 13 – Comparison of different failure modes: (a) cohesive; (b) adhesive.

The results indicate that the AE technique is suitable for obtaining a clearer insight into the debonding phenomenon and fracture propagation in laboratory tests and has potential for on-site health monitoring through debonding detection. Performing a comprehensive experimental program for a better understanding of the advantages of the technique and establishing correlations between fracture properties and AE outputs is necessary. Moreover, development of methods and algorithms for exact damage localization, background noise isolation and use of noncontact-based sensors are to be further investigated.

5. CONCLUSIONS

Three full-field measurement and nondestructive testing technique were used in this study for characterization of debonding and fracture progress as well as bond quality assessment in FRP-strengthened masonry components.

The active IR thermography technique was used for assessing the bond quality and degradation due to environmental conditions. A quantitative IR thermography method was adopted for evaluating the delamination in FRP-strengthened masonry elements. Progressive FRP delamination was observed, with the aim of IR thermography, in the specimens after exposure to environmental conditions. The size of delaminated areas was evaluated quantitatively with the adopted IR thermography method and the results were presented. The obtained results showed the applicability of IR thermography technique in quality assessment of bond in durability studies for research purposes. However, application of this technique for field assessment of strengthened structures remains open with issues such as far-field assessments or assessment of strengthened elements with rendering. Adaptation and development of advanced algorithms for better measurement and detection of bond defects are also to be further studied.

The digital image correlation technique was used for full-field measurement of FRP deformation during debonding tests. The evolution of strains during the shear debonding tests was measured with the DIC technique. Large transversal strains were observed near the loaded end close to failure of the specimens, further confirming the three-dimensional nature of the bond behavior. From the strain profiles, it was possible to extract the bond-slip law in the system under study.

The AE technique was applied to detect and characterize fracture and crack propagation during the debonding tests. The results showed that AE output can be efficiently used for investigation and interpretation of the fracture process during debonding. AE data, and more specifically the detected AE energy, was applied to characterize the different failure modes. The effect of failure mode on the AE outputs was significant. The results indicate that the AE technique is suitable for obtaining a clearer insight into the debonding phenomenon and fracture propagation in laboratory tests and has potential for on-site health monitoring through debonding detection.

6. REFERENCES

ARAMIS. *ARAMIS user manual- Software- v6.0.2-6* (2009).

Carloni, C. & Subramaniam, K. V, FRP-Masonry Debonding: Numerical and Experimental Study of the Role of Mortar Joints, Journal of Composites for Construction, 16(5), 581–89 (2012).

Carrara, P., Ferretti, D. & Freddi, F., Debonding behavior of ancient masonry elements strengthened with CFRP sheets, Composites Part B: Engineering, 45(1), 800–810 (2013).

CNR-DT 200, Guide for the design and construction of externally bonded FRP systems for strengthening existing structures. National Research Council, Rome (2004).

Dohnalek P, Environmental durability of FRP bond to concrete subjected to freeze-thaw action., Master Thesis, MIT (2006).

Ghiassi, B., Marcari G., Oliveira, D.V., Lourenço, P.B., Numerical analysis of bond behavior between masonry bricks and composite materials, Engineering Structures, 43, 210–20 (2012).

Ghiassi, B., Durability analysis of bond between composite materials and masonry substrates, Ph.D. Thesis. University of Minho, Guimaraes (2013a).

Ghiassi, B., Xavier, J., Oliveira, D.V., Lourenço, P.B., Application of digital image correlation in investigating the bond between FRP and masonry, Composite Structures, 106, 340–49 (2013b).

Ghiassi, B., Silva, S.M., Oliveira, D.V., Lourenço, P.B., Bragança, L., FRP-to-Masonry Bond Durability Assessment with Infrared Thermography Method. Journal of Nondestructive Evaluation. doi:10.1007/s10921-014-0238-8 (2014a).

Ghiassi, B., Verstrynge, E., Lourenço, P.B., Oliveira, D.V., Characterization of debonding in FRP-strengthened masonry using the acoustic emission technique, Engineering Structures, 66, 24–34 (2014b).

Grosse, C.U. & Ohtsu, M.. *Acoustic emission testing - basics for research - applications in civil engineering*, Springer (2008).

Kralj, B., Pande, GN., Middleton, J., On the mechanics of frost damage to brick masonry. Composite Structures 41(1), 53-66 (1991).

Lai, W.L., Kou, S.C., Poon, C.S., Tsang, W.F., Lee, K.K., A durability study of externally bonded FRP-concrete beams via full-field infrared thermography (IRT) and quasi-static shear test, Construction and Building Materials, 40, 481–91 (2013).

Maldague, X., Theory and practice of infrared technology for nondestructive testing. Wiley-Interscience, John Wiley&Sons Inc. (2001).

Oliveira, D.V., Basilio, I. & Lourenço, P.B., Experimental Bond Behavior of FRP Sheets Glued on Brick Masonry. Journal of Composites for Construction, 15(1), 32-41 (2011).

Pan, B., Qian, K., Xie, H., Asundi, A., Two-dimensional digital image correlation for in-plane displacement and strain measurement: a review. Measurement Science and Technology. 20(6)2001, doi:10.1088/0957-0233/20/6/062001 (2009).

Sousa, A.M.R, Xavier, J., Vaz, M., Morais, J., Filipe, V.M.J., Cross-correlation and differential technique combination to determine displacement fields. Strain, 47(S2):87-98 (2011).

Sutton, M.A., Orteu, J.J., Schreirer, H., Image correlation for shape, motion and deformation measurements: Basic concepts, theory and applications. Springer (2009).

Tashan, J. & Al-mahaidi, R., Investigation of the parameters that influence the accuracy of bond defect detection in CFRP bonded specimens using IR thermography. Composite Structures, 94(2), 519–31 (2012).

Valluzzi, M.R. Oliveira, D.V., Caratelli, A., Round Robin Test for composite-to-brick shear bond characterization. Materials and Structures, 45(12), 1761–91 (2012).

Verstrynge, E. Schueremans, L., Van Gemert, D., Wevers, M., Monitoring and predicting masonry's creep failure with the acoustic emission technique. NDT & E International, 42(6), 518–23 (2009).

Xavier, J., Sousa A.M.R., Morais J.J.L., Filipe V.M.J., Vaz M., Measuring displacement fields by cross-correlation and a differential technique: experimental validation. Optical Engineering, 51(4), 43602 (2012).